Role of GLP1-receptor-mediated α-β-cell communication in functional β-cell heterogeneity.

Authors: Nirmala V. Balasenthilkumaran[#1], Lidija Križančić Bombek[#2], David Ramirez[1], Maša Skelin Klemen[2], Eva Paradiž Leitgeb[2], Jasmina Kerčmar[2], Jan Kopecky[2], Yaowen Zhang[1], Annanya Sethiya[1], Adam Takaoglu[1], Divya Prabhu[1], Aining Fan[1], Shravani Vitalapuram[1], Jurij Dolenšek[2], Marko Gosak[2], Richard KP Benninger*[3], Andraž Stožer*[2], Vira Kravets*[1,4].

[#]equal contributions, *corresponding authors.

[1] Department of Bioengineering, Jacobs School of Engineering, University of California San Diego, San Diego, CA, United States of America.
[2] Institute of Physiology, Faculty of Medicine, University of Maribor, Maribor, Slovenia.
[3] Department of Bioengineering, Barbara Davis Center for Diabetes, Aurora, Colorado, United States of America, Barbara Davis Center for Childhood Diabetes, University of Colorado Anschutz Medical Campus, Aurora, Colorado, United States of America.
[4] Department of Pediatrics, School of Medicine, University of California San Diego, San Diego, CA, United States of America.

Abstract

While the islet β-cells were traditionally viewed as a singular functional entity, findings of 1970's and up until recent years, reveal that individual β-cells differ in their calcium dynamics and insulin secretion, forming distinct subpopulations that together maintain glucose homeostasis. However, the underlying mechanisms driving functional β-cell heterogeneity are still not fully understood. Here, we aimed to investigate how paracrine signaling, specifically GLP-1R mediated α-β-cell communication shapes functional β-cell heterogeneity. To address this question, we sought to understand how β-cell function and heterogeneity are altered when the α- to β-cell communication was inhibited via GLP1-R antagonist, exendin-9. To this end, we utilized confocal imaging to record calcium response in isolated islets from GCaMP6s mice and in islets from pancreatic slices from C57Bl6 mice, both before and after the application of exendin-9. We found that inhibiting α-β-cell communication prolonged the response-time, increased 1st phase heterogeneity, and decreased the peak of the 1st phase islet's response. Additionally, it reduced 2nd phase oscillation frequency and 2nd phase heterogeneity, thereby enhancing 2nd phase coordination across β-cells. These changes in oscillation frequency were also found to be more pronounced in α-neighboring β-cells. Additionally, we also found that inhibiting GLP1-R mediated α-β-cell communication disrupted the temporal consistency and α-cell proximity of 1st responder and hub-cell functional β-cell subpopulations in the islet.

Keywords:

GLP1-R, α-β communication, β-cell heterogeneity, diabetes, α-cells, β-cell function

Introduction

Diabetes Mellitus is an endocrine disease that is characterized by an increase in blood glucose levels, primarily resulting from decreased insulin secretion by the β-cells in the islets of Langerhans in the pancreas. The β-cells within the pancreas exhibit differences in functional characteristics, transcriptomic profiles, protein expression, gap junction coupling, and insulin release (1-5). These variations result in a heterogeneous response to glucose stimulation,

leading to the existence of distinct subpopulations of β-cells within the islet. We and others have previously shown the existence, temporal and spatial stability of unique functional β-cell subpopulations within the islet (6-8). Recent studies have tried to identify markers that could separate β-cell subpopulations. PSA-NCAM-expressing and Fltp-Venus positive β-cells have been shown to exhibit enhanced insulin secretion and improved overall cell function (5; 9; 10). However, these markers are not always linked to β-cell functionality, and the mechanisms underlying the existence of these functional β-cell subpopulations within the islet remain poorly understood (9).

The islets of Langerhans in the pancreas also comprises of glucagon secreting α-cells, and somatostatin secreting δ-cells, which interact with one another through paracrine signaling, playing a crucial role in maintaining islet function and survival (11-13). δ-cells have a soma and filopodia-like structure and release somatostatin, which binds to the somatostatin receptors on β- and α- cells and suppress insulin and glucagon release (14-16). Conversely, glucagon secreted by α-cells is sensed by glucagon and GLP-1 receptors (Gcg-R, GLP-1R) on β-cells, enhancing glucose-stimulated cyclic AMP and calcium ([Ca^{2+}]) production, and insulin secretion (17; 18). Since intra-islet signaling is predominantly mediated through paracrine and electrical interactions, β-cells located closer to α- and δ- cells are likely to be more strongly influenced, contributing to greater heterogeneity in their responses. (11; 19-22). Moreover, glucagon is crucial for maintaining glucose homeostasis in the body, and α-cells have been shown to become dysfunctional during both T1D and T2D and overproduce glucagon, further contributing to the pathophysiology of diabetes (19; 23-25). We have previously shown that immune cells preferentially interact with α-cell-rich regions of an islet, and α-cells also express more HLA-1 and IL-1β in the islet during T1D (26-28). Understanding the extent to which α-cells influence β-cell function and heterogeneity in healthy conditions would help us better understand intra-islet signaling and diabetes pathophysiology.

During glycolysis, β-cells generate intracellular ATP, which binds to and closes ATP-sensitive potassium channels, causing membrane depolarization. This depolarization triggers the opening of voltage-gated calcium channels, leading to an increase in intracellular [Ca^{2+}] and subsequent insulin release. The insulin release hence correlates with the [Ca^{2+}] response, and both exhibit a biphasic pattern with a well-defined transitional first phase followed by a steady and oscillatory second phase in both rodents and humans (29-33). As β-cells are electrically excitable and coupled to their neighbors via connexin36 (cx36) gap junctions, their electrical activity propagates from one cell to another across the islet, resulting in a coordinated response to glucose stimulation (34-36). The first phase of an islet's response can be characterized by measuring the amplitude and time of response, which vary among individual cells (6). The oscillatory second phase can be characterized by quantifying the oscillation frequency, active time or time lag (37). Finally, the coordination of response can be quantified by constructing and evaluating functional networks, where β-cell pairs within an islet are linked based on the coordination of calcium dynamics (7; 38; 39). The extent to which these parameters of β-cell function are influenced by α-cells remains unclear.

Here, we attempt to investigate the GLP1-R mediated role of α-cells in the regulation of β-cell function and heterogeneity and address how they influence the islet's first and second phases of the glucose-stimulated calcium response by pharmacologically inhibiting the GLP-1 receptor in β-cells using the GLP-1R antagonist exendin-9/39 (ex-9), thereby inhibiting α-β cellular communication. Additionally, we explore how α-cells contribute to defining and maintaining the functional subpopulations within an islet.

Results

GLP1-R signaling speeds up β-cell activation, and enhances strength of the 1st phase [Ca^{2+}] response.

We first sought to investigate the spatial location of cells responding first vs those that respond last to glucose elevation in the islet. The 1st responder β-cells (1st responders) were identified as a functional subpopulation of β-cells that drive the islet's 1st phase [Ca^{2+}] response to high glucose stimulations (6). For this we recorded [Ca^{2+}] dynamics in the live islets and then fixed and post-stained these islets for insulin and glucagon (**Fig.1 A**). As previously defined, we considered first responders to be the 10% of the islet β-cells with the fastest time of response (T_{resp}), and last responders to be the 10% of the islet β-cells with the slowest T_{resp} (6). We found that the 1st responders were located on average, at approximately 80% of the islet radius from the center, positioning them closer to the periphery of the islet than to the core (see **Fig. 1B**). Interestingly, in mouse islets alpha cells are most of the time located at the islet periphery. Hence, we wondered whether 1st responder β-cells would be found in the α-cell-rich neighborhoods of the islet. Indeed, in the isolated islets, we observed that 1st responders have significantly higher α-cell presence in their neighborhoods when compared to last responders ($p = 0.0067$) (see **Fig. 1C**).

GLP1-R signaling amplifies 1st phase peak amplitude of beta cell's response to glucose: We then thought to explore whether there is a functional relationship between α-cells and β-cell responses in the first phase of [Ca^{2+}] dynamics, aside from the proximity relationship described above. We tested to what extent the GLP1-R mediates α-β cell communication in the first phase of [Ca^{2+}] response of the islet. Prior to imaging, pancreatic islets were incubated for 1 hour in low glucose. As depicted in **Fig. 1D**, the islets were placed in 2mM glucose for 10 minutes, followed by high glucose stimulation in 11mM glucose for 20 minutes. Next the islets were treated with 2mM glucose for 20 minutes and stimulated again by 11mM glucose for another 20 minutes. In the experimental group, α-β cell communication was inhibited by the addition of 100nM ex-9 for the second stimulation (during both low and high glucose incubations) (See Materials and Methods for detailed description).

In the experimental (ex-9 treated) group we found a greater drop in the 1st phase peak amplitude, compared to the control group ($p = 0.0028$) (**Fig. 1E**). It was quantified by the difference in first-phase peaks between the 1st and 2nd stimulations within the same islet.

GLP1-R signaling has a mild effect on the 1st responder consistency: We next aimed to investigate if the function of 1st responders is affected by inhibition of the GLP1-R cell communication. In isolated islets, we observed that a significantly higher percentage of β-cells identified as 1st responders during the 2nd stimulation were either the same cells or in close proximity (1st nearest or 2nd nearest neighbors) to the original 1st responders from the 1st stimulation (same cell cluster) ($p = 0.0006$) (See **Fig. 1F**). This pattern, however, was disrupted with the addition of ex-9 addition ($p = 0.2031$), aligning with our previous findings (40). Interestingly, in islets within the pancreatic slices we did not observe a significant temporal consistency for both control and ex-9 treated islets (which will be discussed next). Therefore, α-cells play a role in aiding the 1st responders in maintaining their spatio-temporal consistency in isolated islets, but this effect is weak, and not prominent.

GLP1-R signaling affects beta cell response time in pancreatic slices: Since it has been previously reported that enzymatic digestion during the islet isolation may affect the number of

α-cells on the islet periphery, we also tested GLP1-R and alpha cell proximity effects in islets from live pancreatic slices. This platform offers the advantage of the unperturbed α-cell numbers on the islet periphery. **Fig 2 A** shows an example of [Ca^{2+}] staining of the islet, where brightest areas indicate vasculature, as well as immunofluorescence of the same islet within the slice. We observed a similar α-cell proximity correlation with the fastest T_{resp} to glucose, as we saw in isolated islets. However, the difference was not statistically significant between 1st and last responders ($p = 0.5974$) (**Fig. 2 B**). The stimulation protocol for slices (**Fig. 2 C**) was the same as for the isolated islets, aside from the calcium dye used, as opposed to genetically-encoded calcium indicator in isolated islets.

GLP1-R signaling speeds up and non-significantly enhances β-cell response in pancreatic slices: We then quantified islet-average changes in the 1st phase response (peak amplitude, **Fig. 2 D**) and activation time (T_{resp}) after (see **Fig. 2 E**). The peak amplitude was lower upon the GLP1-R inhibition, similarly to the isolated islets, however in slices this effect was not significant (**Fig. 2 D**). On average in the subsequent glucose stimulation the response time was shorter for the control group and longer for ex-9 treated islets ($p < 0.0001$) (**Fig. 2 E**). Cells that did not respond in either of the two stimulations were excluded from analysis, and for cells that were unresponsive in either of the two stimulations, a T_{resp} of 20 mins was assigned for that stimulation.

Upon GLP1-R inhibition we found that the 1st responders appeared less near the alpha cells, as opposed to 1st responders in the unperturbed conditions ($p = 0.1070$) supporting our hypothesis that α-cells help define and maintain the 1st responder subpopulation (**Fig. 2F**).

GLP1-R signaling decreases the heterogeneity of 1st phase β-cell response in the islet.

We next aimed to investigate if GLP1-R mediated α-β cell communication influences the heterogeneity of β-cell response within an islet. In isolated islets, we first plotted the distribution of T_{resp} of all the beta cells in each islet, centered around the median T_{resp} (**Fig. 3 A**). Islet with the wide distribution (red) and narrow distribution (blue) of the responsiveness during the first phase are shown in **Fig. 3 A**. To assess the spread of T_{resp} within an islet, we then plotted the islet-wise width (distribution variance) for the T_{resp} for both the 1st and 2nd stimulations (**Fig. 3 B**). We observed a broader distribution upon ex-9 addition (see **Fig. 3 B, C**), consistent with our previous findings (40). **Figure 3 C** simply summarizes the data presented in **Fig. 3 B**, showing that the increase in heterogeneity of T_{resp} in ex-9 stimulations was significantly different than in control stimulations ($p = 0.0259$), and suggesting that inhibition of GLP1-R mediated α- β-cell communication enhances the heterogeneity of β-cell response.

GLP1-R signaling increase the speed of [Ca^{2+}] signal propagation in the 1st phase: As we previously found a decrease in the 1st phase response on ex-9 addition , we reasoned that this could be attributed to a decrease in the strength of [Ca^{2+}] signal generation by the 1st responders, and that the [Ca^{2+}] signals do not propagate as fast as they used to. To test this, we created an automated, bias-free 'domain' recognition algorithm that groups individual β-cells in an islet into different domains as shown in **Fig. 3 D** (see Supplementary **Figure S1** for more information on how the domains were determined). Each domain consists of a local 1st responder which initiates the 1st phase [Ca^{2+}] response which propagates the electrical signal to all the other β-cells in the domain. In other words, the β-cells in a domain are excited by the same 1st responder. The slope of the distance to the 1st responder vs time of response of each beta cell belonging to the individual domain indicated the *speed* of the calcium signal (**Fig. 3 E**). In isolated islets, we observed that the speed of signal propagation in a domain decreased

when the islets were treated with ex-9 ($p < 0.0001$), while no significant changes were noted in the control experiments (See **Fig. 3 F**). Additionally, we observed an increase in domain size during the 2nd stimulation in control experiments ($p = 0.0169$), suggesting larger domains upon repeated stimulation. In contrast, no significant changes in domain area were observed when the islets were treated with ex-9 (see **Fig. 3 G**), further supporting our hypothesis that the decrease in $[Ca^{2+}]$ signal generation due to ex-9 addition, leads to slower $[Ca^{2+}]$ signal propagation, which in turn leads to the formation smaller independently responding domains.

GLP1-R signaling amplifies the oscillatory (second phase) $[Ca^{2+}]$ response.

Number of α-cells positively correlates with frequency of $[Ca^{2+}]$ oscillations in β-cells: We quantified the frequency of $[Ca^{2+}]$ oscillations during the 2nd phase $[Ca^{2+}]$ response to glucose, utilizing a custom MATLAB-routine involving signal filtering and peak-detection to determine oscillation frequency (see Materials and Methods for detailed description of the algorithm). After functional imaging, islets were fixed, stained for hormones, and the same focal plane as well as +/- 10 micrometers above and below were imaged for immunofluorescence assessment. We used Imaris softwares to segment the islet cell types based on the immunofluorescence (**Fig. 4 A**). In most islets with a higher α-cell count, we observed a higher oscillatory frequency (See **Fig. 4 B**). We then observed a positive correlation of the oscillation frequency with the α-cell count, aligned with previously published findings, further supporting the role of α-cells in enhancing β-cell oscillatory frequency (41).

To test whether GLP1-R signaling in the islet influences the oscillatory $[Ca^{2+}]$ response of β-cells, we applied ex-9 as before, focusing on the analysis windows during the 1st and 2nd stimulations **Fig. 4 A**. Consistent window sizes were maintained for both stimulations, with each window beginning just prior to the 1st peak of the 2nd phase response and extending until either when the glucose was switched from 11 mM to 2mM or the end of the experiment. To ensure accurate peak detection and frequency calculation, we calculated the signal to noise ratio (SNR) of each cell's $[Ca^{2+}]$ trace within the analysis windows and only included the cells with var(signal) > 0.25*σ(noise) in both windows (See Materials and Methods for details). We tested multiple thresholds and found that the results remained consistent, regardless of the threshold used. We observed a significant change in oscillation frequency during the 2nd stimulation between ex-9 treated and control islets. Specifically, a significant decrease ($p < 0.0001$) in frequency was observed after ex-9 treatment (see **Fig. 4 C**), whereas control islets exhibited a frequency increase, highlighting the importance of α-β communication in regulating the 2nd phase $[Ca^{2+}]$ response.

Proximity to α-cells affects the magnitude of the β-cell's response to ex-9: We next sought to determine if the β-cells situated closer to α-cells are influenced more than those without α-cell neighbors by GLP1-R inhibition. To do this, we overlaid the $[Ca^{2+}]$ time series recordings with their corresponding IF images (see **Fig. 4 E and 4 G**), computed the α-cell volume fraction in the immediate neighborhood of each β-cell in an islet, and categorized the β-cells with α-cell volume fraction greater than zero to be α-neighboring and all other β-cells with volume fraction equal to zero to be non α-neighboring. We then quantified the change in oscillatory frequency for both control and ex-9 treated islets. Overall, the oscillatory frequency increased in control and decreased in ex-9 treated islets (see **Fig. 4 D**). Notably, we observed a significantly greater increase in frequency ($p < 0.0001$) in α-neighboring β-cells than non α-neighboring β-cells in control experiments (see **Fig. 4 F**). Similarly, on ex-9 treatment, α-neighboring β-cells exhibited a significantly greater ($p = 0.0002$) decrease in frequency than non α-neighboring β-cells (see

Fig. 4 H). These findings suggest that α-cells exert both a broad, and a stronger localized modulatory influence on β-cell dynamics during the 2nd phase of the [Ca^{2+}] response.

The islet-wide functional connectivity is increased under GLP1-R inhibition due to decrease in the heterogeneity of [Ca2+] responses of beta cells.

As α-cells influence the oscillatory phase of β-cell response, we next sought to investigate if they also affect the functional connectivity of islets during the 2nd phase, including the β- hub cell subpopulation. We generated functional β-cell networks for the 1st and 2nd stimulations using a combination of variable-threshold and variable K_{avg} method (see Materials and Methods for detailed description). In short, we fixed the average number of functional links (K_{avg}) of each islet's network to 8 in the 1st stimulation and used the resulting threshold to construct its network in the 2nd stimulation. **Fig. 5 A** shows the network representation of a control islet during both stimulations, while **Fig. 5 B** depicts the same for an islet treated with ex-9. As shown in **Fig. 5 C**, we observed a slight decrease in functional connectivity in control islets and an overall increase in connectivity in ex-9-treated islets during the 2nd stimulation ($p < 0.0001$). Given the disproportionate increase in 2nd stimulation oscillatory frequency among α-neighboring β-cells (as was shown in **Fig. 4 F**), we hypothesized that this leads to greater heterogeneity in frequency distribution and hence a reduced coordination. Conversely, ex-9 treatment—by decreasing oscillatory frequency (as was shown in **Fig. 4 G**) may reduce heterogeneity and enhance coordination. To test this, we calculated the percentage change in the spread (standard deviation) of oscillation frequency between the 1st and 2nd stimulations (**Fig. 5 D**). Indeed, the control islets showed an increase in standard deviation and ex-9-treated islets showed a decrease. The difference between the two conditions, however, was not statistically significant ($p = 0.4857$).

GLP1-R mediated α-β cell communication helps maintain hub-cell temporal consistency: Hub-cells were identified as functional β-cell subpopulation that coordinate β-cell oscillations in the islet (7). As previously defined, we considered hub-cells to be the β-cells with greater than 60% of the node degree distribution, obtained by normalizing each cell's node degree with the maximum degree in that islet (42). In islets from slices, we observed that a higher percentage of β-cells identified as hub-cells during the 2nd stimulation were either the same cells or in close proximity (1st nearest or 2nd nearest neighbors) to the hubs from the 1st stimulation (same cell cluster), when compared to the hubs in the 2nd stimulation ($p = 0.1250$) (see **Fig. 5 E**). This pattern, however, was disrupted with the addition of ex-9 addition (see **Fig. 5 F**). We also observed a significant decrease in temporal consistency on ex-9 addition. Therefore, α-cells aid hub cells in maintaining their temporal consistency.

GLP1-R inhibition leads to loss of hub cells from the α-cell-rich neighborhoods: As we observed a decrease in hub-cell temporal consistency on ex-9 addition, we next aimed to investigate whether the hub-cell proximity to α-cells is altered by ex-9 addition. Firstly, we observed that hub-cells displayed a higher α-cell volume fraction in their immediate neighborhood, however it was not significantly different ($p = 0.5781$), compared to non-hub cells (see **Fig. 5 G**). To assess changes in location of hub cells with respect to α-cells, we calculated the fold change in α-cell volume fraction associated with hub cells between the 1st and 2nd stimulations. In control islets, this fold change significantly increased ($p = 0.0571$), whereas it decreased in ex-9–treated islets (**Fig. 5 H**). As there is a change in the proportion of hub-cells that are α-neighboring upon ex9 treatment, we next sought to investigate how the relative connectivity rank of α-neighboring β-cells compared to the rest of the islet is altered. To do this, we computed the change in percentile rank of the node degree (2nd – 1st stimulations) for α-neighboring β-cells. We found

that this relative connectivity significantly increased in control islets ($p < 0.0001$) but decreased in ex-9–treated islets (see **Fig. 5 I**), suggesting that GLP1-R mediated α-β communication may enhance relative connectivity in α-neighboring β-cells.

Discussion

While previous studies suggest that α-cells enhance β-cell function, they primarily focus on studying the effects of glucagon signaling by examining β-cell function in the absence of glucagon and GLP-1 receptors (17; 18; 43). In contrast, we pharmacologically inhibit α-β cell communication within the islet using ex-9, allowing us to assess the extent to which an islet's function is influenced by GLP1-R function. We demonstrated that the 1st phase strength, 2nd phase oscillation frequency, and 2nd phase functional connectivity are all significantly affected when β-cells do not utilize their GLP1-R. We also show that these effects are more predominant in those β-cells that are neighboring α-cells.

Why do α-cells decrease the time-of-response of β-cells in the 1st phase?

We first demonstrated that α-cells amplify the 1st phase response in β-cells, and decrease the time taken for β-cells to respond to high glucose stimulations (see **Fig. 1 E** and **2 E**). Glucagon, secreted by the α-cells binds to the GLP-1 and glucagon receptors in the β-cells (17; 18; 44; 45). However, recent studies show that α-β- glucagon signaling is primarily achieved via the GLP-1R receptors, as Gcg-R knockout mice have been shown to exhibit normoglycemia (44-46).

When glucagon binds the GLP1 receptors, it interacts with the Gαs subunit, which subsequently activates adenyl cyclase, resulting in cAMP production (47). cAMP activates both the protein kinase A (PKA) and Epac2A signaling pathways, amplifying insulin secretion (48). PKA phosphorylates key exocytotic proteins, facilitating [Ca^{2+}] release and insulin granule exocytosis, while also targeting the Kir6.2 subunit in the K_{ATP} channels to promote closure and membrane depolarization (49-51). Epac2A activates Rap1 and promotes the recruitment of the insulin granules to the plasma membrane (52; 53). Hence, the observed enhancement of the 1st phase [Ca^{2+}] response could be attributed to increased activity of L-type voltage dependent [Ca^{2+}] channels (VDCCs) which increase voltage dependent [Ca^{2+}] currents, as the inhibition of these channels was shown to reduce [Ca^{2+}] response (54; 55). When [Ca^{2+}] enters the islet through VDCCs, the resultant increase in cytoplasmic [Ca^{2+}] triggers additional [Ca^{2+}] release from the endoplasmic reticulum, via [Ca^{2+}]-induced-[Ca^{2+}] release (CICR), which has previously shown to be facilitated by exendin 4, a GLP-1 agonist (56; 57). Inhibition of Epac2A and PKA diminishes exendin-4-induced CICR, while their activation restores it—suggesting a potential mechanism through which GLP-1 signaling amplifies Ca^{2+} dynamics and insulin secretion (58).

GLP-1(7-36) amide has been shown to increase glucose responsiveness, and first phase [Ca^{2+}] response. Addition of forskolin, an adenyl cyclase activator has shown to increase intracellular cAMP, amplifying [Ca^{2+}] response, and elicited β-cell response at 6mM low glucose conditions in an EPAC-2 independent manner (59; 60). Hence, we speculate that due to increased cAMP concentrations in the presence of glucagon, β-cells more readily respond to glucose stimulations, resulting in a faster and more amplified response. In the presence of a GLP1-R antagonist such as ex-9, there is a significant decrease in cAMP production, and therefore β-cells are less ready to respond to glucose stimulations, resulting in a decreased [Ca^{2+}] response in the 1st phase (61).

How do α-cells decrease β-cell heterogeneity in the 1st phase?

The 1st phase [Ca^{2+}] response has previously been shown to originate in β-cells with elevated excitability (6). Time delays in activation among β-cells reflect electrical coupling, with [Ca^{2+}] waves propagating across the islet (62). Here we demonstrated that GLP1-R mediated paracrine signaling mildly speeds up the T_{resp} of the islet and enables the β-cells closer to α-cells to respond faster to glucose stimulations (see **Fig. 2 E**). Additionally, we observed an increase in β-cell heterogeneity upon blocking α-β cell communication (see **Fig. 3 B**, **3 C**), and a decrease in the amplitude of 1st phase [Ca^{2+}] response (see **Fig. 1 E** and **2 D**) on ex-9 treatment, which likely reflects a decrease in the strength of [Ca^{2+}] signal generated by β-cells. We speculate that this diminished signal strength is increasing heterogeneity in T_{resp}. While gap junction coupling is another factor that could influence the speed of [Ca^{2+}] wave propagation (34), β-cell activity was recorded only 20 mins after ex-9 treatment, a timescale insufficient to induce significant changes in cx36 expression and gap junction coupling.

Why do α-cells increase the frequency of β-cell [Ca^{2+}] oscillations in the 2nd phase?

We demonstrated that second-phase [Ca^{2+}] oscillation frequency decreases following ex-9 treatment, while it increases under control conditions (see **Fig. 4 D**). Interestingly, this change in oscillation frequency was more pronounced in α-neighboring β-cells (see **Fig. 4 F** and **4 H**). An increase in oscillation frequency has previously been reported following the addition of cAMP agonists (63; 64). GLP-1 and glucagon have also been shown to induce cAMP oscillations, which leads to an increase in [Ca^{2+}] oscillations (47; 65). Moreover, cAMP oscillations in β-cells have been found to synchronize with [Ca^{2+}] activity and modulate both PKA and Epac2A signaling (47; 66). We suggest that the paracrine effects of glucagon signaling are likely stronger in α-neighboring β-cells, resulting in more pronounced frequency changes upon GLP1-R inhibition. As discussed in the previous section, ex-9 treatment may reduce cAMP oscillations, thereby contributing to the observed decrease in 2nd phase [Ca^{2+}] oscillations (61).

How does α- β communication impact the different functional β-cell subpopulations?

We identified that 1st responders—a functional β-cell subpopulation triggering 1st phase islet's response to glucose—are primarily located at the islet edge, often near α-cells, and show a higher α-cell volume fraction in their immediate vicinity compared to last responders (see **Fig. 1 B, 1 C, 2 B**). These cells display the fastest T_{resp}, likely due to paracrine signaling, as glucagon may elevate cAMP levels more effectively in these cells, enhancing their responsiveness to glucose. To determine whether their behavior is driven by α-cell proximity or intrinsic traits, ex-9 was used to inhibit α-β signaling. Previously, a large proportion of 1st responders were found to contain a readily releasable insulin pool, and they also exhibit higher vitamin B6 production and lower K_{ATP} conductance, supporting the idea of cell-autonomous, intrinsic properties of this subpopulation (6; 67; 68). Ex-9 slightly reduced the temporal consistency of 1st responders, suggesting a role for α-cell interactions (see **Fig. 1 F, 2 F**). However, the effects were not significant in islets from slices. Additionally, as cAMP/PKA signaling promotes K_{ATP} channel closure, ex-9 may increase conductance and affect membrane excitability, suggesting that behavior of the first responders stems from both cell-autonomous and non-autonomous (paracrine) factors (51; 61).

We identified that hub cells—a functional β-cell subpopulation previously characterized as the most coordinated in the islet—lose their temporal consistency and appear less frequently near the α-cells upon ex-9 treatment (see Fig. 5 E, 5 H). Hub cells, typically located in the islet core, have been shown to display increased gap junctional conductance and metabolism through elevated glucokinase expression, with recent studies emphasizing the importance of metabolic

coupling and intrinsic properties in defining hub identity (7; 42). Ex-9 reduces cAMP levels, an effect likely more pronounced in β-cells neighboring α-cells, which normally experience elevated cAMP due to glucagon signaling (47; 61). cAMP activates PKA, which phosphorylates key components of the electron transport chain, thereby enhancing ATP production, oxidative phosphorylation, and overall metabolic activity (69). Thus, the decline in glucose metabolism in α-neighboring β-cells may underline the reduced temporal consistency of hub cells. Conversely, in the presence of GLP1-R mediated signaling, we observe increased α-cell volume fraction around hub cells, highlighting the importance of cellular metabolism in defining and maintaining hub identity.

Conclusion

Overall, our study emphasizes the importance of GLP-1 receptor and α–β-cell communication in supporting β-cell function and heterogeneity. Several studies have shown how the loss of these specialized functional subpopulations leads to a disproportionate decline in overall islet β-cell performance. Since α–β-cell communication was found to elicit faster β-cell responses, higher 1st phase peak amplitudes, and increased 2nd phase oscillation frequency, designing islets that include both α- and β-cells may offer a more effective strategy for stem-cell-derived islet replacement therapies in the treatment of T1D.

Materials and methods

Ethics Statement: For islet isolation, male and female mice were used under protocols approved by the University of Colorado Institutional Animal Care and Use Committee (IACUC Protocol number: 00024). For pancreatic slices, the protocols used were in accordance with the European and national legislation and approved by the Administration for Food Safety, Veterinary Sector and Plant Protection of the Republic of Slovenia (permit numbers U34401-35/2018-2).

Mouse tissue slice preparation and dye loading: C57BL/6J mice were housed in individually ventilated cages with a 12-hour light/dark cycle and given ad libitum access to standard chow (Ssniff, Soest, Germany). The pancreatic slices were prepared as previously described (70-72). Mice aged 8–20 weeks were sacrificed via CO_2 inhalation followed by cervical dislocation, and a laparotomy was performed to access the abdominal cavity. The common bile duct was clamped at the major duodenal papilla, and 1.9% low-melting-point agarose dissolved in extracellular solution (ECS) (Contains 125 mM NaCl, 26 mM $NaHCO_3$, 6 mM glucose, 6 mM lactic acid, 3 mM myo-inositol, 2.5 mM KCl, 2 mM Na-pyruvate, 2 mM $CaCl_2$, 1.25 mM NaH_2PO_4, 1 mM $MgCl_2$, and 0.5 mM ascorbic acid) was injected into the bile duct to inflate the pancreas. Immediately after the injection, the pancreatic tissue was cooled with ice-cold ECS, extracted from the abdominal cavity, and placed in a petri dish containing ice-cold ECS. Connective tissue and vasculature were removed from the pancreas, and it was cut into 3–5 mm^3 tissue cubes. The tissue sections were then embedded in agarose and sliced into 140 µm sections using a vibratome (VT 1000 S, Leica Microsystems, Wetzlar, Germany). The slices were collected in HEPES-buffered saline (HBS) (Contains 150 mM NaCl, 10 mM HEPES, 6 mM glucose, 5 mM KCl, 2 mM $CaCl_2$, 1 mM $MgCl_2$, titrated to pH 7.4 with 1 M NaOH) and were stained by incubating them at room temperature for 50 minutes on an orbital shaker at 40 rotations per minute in a solution containing 25 µg Oregon Green 488 BAPTA-1 (OGB-1, Invitrogen, Waltham, MA, USA) or 25 µg Calbryte 520 AM (AAT Bioquest, Pleasanton, CA, USA), 3.75 µl dimethyl sulfoxide, and 1.25 µl of 20% (w/v) Pluronic F-127 dissolved in 3.33 ml HBS.

The slices were transferred to a 100 mm petri dish containing fresh HBS with 6 mM glucose for [Ca^{2+}] recordings and were held in place using an anchor. Unless otherwise specified, all chemicals were obtained from Sigma Aldrich (St. Louis, MO, USA).

Isolation of mouse islets: Mice with β-cell-specific GCaMP6s expression (β-GCaMP6s) were generated by crossing MIP-CreER-expressing mice (The Jackson Laboratory) with GCaMP6s-expressing mice (The Jackson Laboratory). Genotypes were verified using qPCR (Transetyx, Memphis, Tennessee, United States of America). The mice were housed in a temperature-controlled facility with a 12-hour light/dark cycle and had continuous access to food and water. CreER-mediated recombination was induced by administering tamoxifen at a dose of 50 mg/kg body weight in corn oil via intraperitoneal injection for five consecutive days. For islet isolation, mice were anesthetized using ketamine/xylazine (80 and 16 mg/kg). A laparotomy was performed to access the abdominal cavity, and the common bile duct was clamped. Collagenase was injected into the bile duct to inflate the pancreas. The inflated pancreas was then surgically excised and digested. The islets were manually picked and attached to glass bottom dishes (MatTek) using Celltak cell issue adhesive (Sigma-Aldrich). They were cultured in RPMI medium (Corning, Tewksbury, Massachusetts, United States of America) containing 10% fetal bovine serum, 100 U/mL penicillin, and 100 mg/mL streptomycin and were incubated at 37°C with 5% CO_2 for 24 to 72 hours before imaging.

Fixing and post-staining of islets: Isolated islets and islets from tissue slices were fixed with 4% PFA. Following permeabilization (0.25% Triton X-100 in blocking buffer) and blocking (5% BSA in PBS), the islets were stained with antibodies for 1 day and imaged the following day. Isolated islets were stained with anti-insulin (eBioscience, 53-9769-82; 1:100 dilution) and anti-glucagon (Bioss, bs-3796R-Cy5; 1:100 dilution) antibodies. Islets from slices were stained with anti-insulin (eBioscience, 53-9769-82; 1:100 dilution), anti-glucagon (eBioscience, 41-9743-82; 1:10 dilution), and anti-somatostatin (eBioscience, 50-9751-82; 1:40 dilution) antibodies.

Glucose stimulation protocol: One hour prior to imaging, the islets or slices were incubated in 2 mM low glucose. Calcium recording was performed at 37°C, starting with a 10-minute exposure to 2 mM low glucose, followed by a high-glucose stimulation at 11 mM for 20 minutes. This was followed by a 20-minute period of starvation in 2 mM low glucose and then followed by a 2nd high-glucose stimulation at 11 mM for another 20 minutes. In the experimental group, 100nM ex-9 was added during the second stimulation (after 30 minutes).

[Ca^{2+}] Imaging: One hour before imaging, the nutrient media in isolated islets was replaced with an imaging solution containing BMHH and BSA (125 mM NaCl, 5.7 mM KCl, 2.5 mM $CaCl_2$, 1.2 mM $MgCl_2$, 10 mM HEPES, and 0.1% BSA titrated to a pH of 7.4) and 2 mM glucose. For [Ca^{2+}] measurements, islets were imaged using either an LSM780 system (Carl Zeiss, Oberkochen, Germany) with a 40× 1.2 NA objective or an LSM800 system (Carl Zeiss) with a 20× 0.8 NA Plan-Apochromat objective. For [Ca^{2+}] imaging, a 488 nm laser was used to excite the GCaMP6s fluorescence. The imaging plane was set at a depth of 10–15 µm from the surface, and time series were acquired at a 1 Hz sampling rate.

A similar protocol was followed for imaging tissue slices. Before imaging, slices were incubated in 2 mM glucose in HBS at room temperature. The slices were then transferred to a recording chamber, where ECS solutions with varying glucose concentrations, depending on experimental conditions, were continuously perfused. For [Ca^{2+}] measurements, slices were imaged using either a Leica TCS SP5 AOBS Tandem II upright confocal system with a 20× 1.0 NA HCX APO L water immersion objective, or a Leica TCS SP5 DMI6000 CS inverted confocal

system with a 20× 0.7 NA HC PL APO water/oil immersion objective, with a 488 nm laser used to excite the calcium-sensitive dye. The imaging plane was set at a depth of 15 µm from the surface, and time series were acquired at a 2 Hz sampling rate with a resolution of 512 × 512 pixels.

Cell Segmentation: Cells were manually segmented from its [Ca^{2+}] imaging time series using the 'Time Series Analyzer V3' plugin in ImageJ (FIJI) (73; 74). A standard deviation-based time-projection was performed on the [Ca^{2+}] time series recording, and regions of interest (ROIs) were manually outlined using the freehand tool. The [Ca^{2+}] response for each ROI was plotted, and cells with calcium signals that did not resemble typical β-cell activity were excluded.

Analysis of [Ca^{2+}] dynamics: [Ca^{2+}] traces were generated by loading an islet's [Ca^{2+}] time series and the ROIs of individual cells in ImageJ, then calculating the mean intensity of each cell at different time points. The time of response was defined as the time at which the [Ca^{2+}] intensity reached half its maximum height attained during high glucose stimulation. This study focuses primarily on two β-cell subpopulations, with the following definitions. 1st responders were defined as the top 10% of the cells with the fastest 1st phase [Ca^{2+}] response, or those with the shortest response time (6). Hub cells were defined as the cells with a degree distribution greater than 0.6, which was in turn computed by dividing the node degree of a cell by the maximum node degree of the islet (42). The [Ca^{2+}] traces also underwent additional pre-processing steps as described in the following sections.

[Ca^{2+}] time series - IF overlay: To determine the positions of α- and β-cells within the islet and correlate these positions with [Ca^{2+}] imaging data, we overlaid the IF image with the [Ca^{2+}] time series recording. IF images were captured as Z-stacks after fixing and post-staining the islets, while [Ca^{2+}] imaging was conducted on a single Z-plane. We compared the different Z-planes of the insulin channel from the IF Z-stack with the backscatter image captured immediately after recording [Ca^{2+}] dynamics in isolated islets. We systematically explored the different Z-stacks to identify the most appropriate Z-plane from the IF data, and subsequently applied scaling, rotation and translation to the IF image to achieve optimal alignment with the backscatter image. Alignment was visually confirmed by ensuring the features such as basement membranes and individual cells matched across both images. The resultant IF image was then used for subsequent analysis. For slices, we used a standard deviation-based time projection of the [Ca^{2+}] time series recording for alignment, instead of the backscatter image for alignment. Additionally, the canvas size of the backscatter and [Ca^{2+}] time series images was enlarged to match the pixel dimensions of the IF image, ensuring proper spatial correspondence.

α-cell volume fraction: In the overlaid IF image, spheres of diameter 25 µm were constructed (in X, Y and Z directions) to represent individual β-cell. The centers of these spheres were defined by the centroids of the ROIs previously identified from the [Ca^{2+}] time series data. For each β-cell, the local α-cell volume fraction was calculated by quantifying the glucagon signal contained within the corresponding sphere and normalizing it to the total volume of the sphere. In cases where the glucagon IF channel exhibited high background or noise, we applied background subtraction and median filtering using ImageJ to improve signal quality prior to analysis. To account for noise, we also set the volume fraction of cells with magnitudes lower than 0.5 to 0.

Consistency analysis: Each β-cell in the islet was mapped to its nearest and second-nearest neighboring β-cells based on spatial proximity (Euclidean distance). We first identified the list of

β-cells belonging to the 1st responder and hub-cell subpopulations during both the 1st and 2nd stimulations. For each subpopulation, we quantified the proportion of 1st responders or hub cells in the 2nd stimulation that were either (i) the same cell, (ii) the 1st nearest neighbor, or (iii) the 2nd nearest neighbor of a 1st responder or hub cell from the 1st stimulation—collectively referred to as belonging to the same "cell cluster.". We also computed the proportion of cells in the 2nd stimulation that were 1st responders or hubs but did not belong to the same cell cluster (i.e., not the same cell or a 1st/2nd nearest neighbor) in the 1st stimulation. In the Results section, we compare cluster-wise consistency across stimulations.

Domain analysis: The positions of the cells in the islet were exported from ImageJ by computing the centroids of the ROIs outlined for each cell. A spatial representation of these cells was then created in Matlab (MathWorks, Natick, United States of America), where they were color-coded based on their T_{resp}. Warmer colors indicated faster response times, while cooler colors indicated slower response times. Each cell was indexed, and a list was generated by sorting the cells according to their response times. Initially, the fastest responding cell was considered the 1st responder, and the relative distances of all other cells to this 1st responder were computed. The cells were then sorted in ascending order of distance. The mean distance between consecutive cells was calculated, and the bin radius was set to three times this mean distance. Cells were categorized into bins based on their distance from the 1st responder. The cells were plotted again and color-coded based on whether their response time increased or decreased relative to the cells in the previous bin. We defined the 1st domain, starting with the 1st responder, moving to the 1st closest bin and manually added cells from this bin whose response time increased compared to the previous bin. We then moved to the next closest bin and repeated this process of adding and removing cells until a list was generated where the coefficient of determination (R^2) value was greater than 0.7 when response time was plotted against distance from the first responder. Cells whose addition negatively affected this regression line were excluded from this domain. Next, the fastest responding cell from the list of cells not yet assigned to a domain was identified, and the process was repeated until all cells were assigned to a domain.

Functional network analysis: Calcium traces corresponding to the second-phase response were pre-processed as previously described (39; 75). The same analysis windows used for frequency analysis (explained in the next section) were also utilized here. A custom MATLAB routine was created to implement functional network analysis. Signals with low signal-to-noise ratios and non-β-cell-like features were excluded. Every cell that had a distinct first and second phase response in either of the two stimulations were included. A band-pass filter was applied to retain frequency components between 0.02 and 0.8 Hz, followed by smoothing with a moving average filter of window size 2. Functional network analysis was performed as previously described (38; 76). We first computed the pairwise Pearson correlation coefficient based on the temporal similarity between the calcium traces of each cell pair and generated a correlation matrix (72; 77). From this, we constructed a functional network with a variable threshold (R_{th}), linking two cells in the network if their Pearson correlation coefficient exceeded the threshold. The average number of links per cell (K_{avg}) (or average node degree) was calculated by dividing the total number of links in the network by the number of cells in the network. For the 1st stimulation in each islet, the threshold was adjusted to achieve an average of approximately 8 links per cell, reflecting realistic β-cell connectivity within the tissue (78). For the 2nd stimulation, we utilized the same threshold from the first stimulation to construct networks and then computed the K_{avg} of these networks. We also tried adjusting the threshold to achieve an average node degree of 6 and 10 links during the 1st stimulation and obtained similar results.

Frequency analysis: The [Ca^{2+}] traces from slices corresponding to the oscillatory 2nd phase were extracted from the overall [Ca^{2+}] signals for each individual cell. Consistent analysis window sizes were maintained across both the 1st and 2nd stimulations for each islet, with the window beginning just prior to the 1st peak of the 2nd phase. A low-pass filter with a frequency of 0.03001 Hz was applied to isolate the slow frequency component, which was then subtracted from the raw data within the second phase window to obtain a 'residual' time course. This residual was detrended, centered near the x-axis, and smoothed using a 4th order Butterworth filter. A high-pass filter (cutoff: 1 Hz) was subsequently applied to reduce low-frequency noise. Peaks were identified as regions where the signal exceeded the threshold defined by mean(residual) + 2×std(residual) (79). The time intervals between consecutive peaks were measured to calculate the oscillation frequency.

Statistical analysis: All statistical analysis was performed using GraphPad Prism (GraphPad, Boston, United States of America). Data was reported as ± SEM. The differences were considered to be statistically significant for $p < 0.05$. The tests used for evaluating statistical significance between results are mentioned in the figure captions.

Acknowledgements: We thank Dr. Stephan Speier of Technical University of Dresden, Germany, and his team for facilitating the pancreatic tissue slice training for Dr. Kravets and their valuable comments on the experimental design of this work. We also thank Dr. Marko Sterk of the University of Maribor, Slovenia for their involvement in developing the network analysis algorithm.

Data availability statement:

The MATLAB scripts used for analysis, and the raw data obtained will be uploaded to a repository, and the link to the repository will be included in the manuscript if/once accepted to publish.

Figure captions:

Figure 1. Variation in T_{resp} with α-cell proximity and ex-9 addition in isolated islets (A) Schematic representation of the [Ca^{2+}] time series projection snapshot and IF image overlay in isolated islets **(B)** Comparison of the location of 1st and last responders in the islet relative to the center of the islet (Mann-Whitney test was used for statistical analysis) **(C)** Comparison of cell-wise α-cell volume fraction of 1st and last responders in the 1st stimulation (n = 29 1st responders and n = 29 last responders from 5 islets) (Mann-Whitney test was used for statistical analysis and outliers were removed using ROUT method(Q =1%)) **(D)** Experimental protocol and representative [Ca^{2+}] time course of an ex-9-treated GCaMP6s isolated islet, along with representative islet snapshots at different time points **(E)** Comparison of the decrease in islet-average 1st-phase peak amplitude during the 2nd stimulation in control and ex-9-treated islets (n = 7 control islets, and n = 11 ex-9-treated islets) **(F)** Comparison of the islet-wise proportion of 1st responders in the 2nd stimulation that were part of the same cell, 1st nearest neighbor, or 2nd nearest neighbor (same cell cluster) versus the proportion of 1st responders who were different cells in the 1st stimulation, in control and ex-9-treated islets (n = 19 control islets and n = 8 ex-9-treated islets) (Wilcoxon matched-pairs signed-rank test was used for statistical analysis) (Experiments were performed in isolated islets for the data presented in this figure)

Figure 2. Variation in T_{resp} with α-cell proximity and ex-9 addition in islets from pancreatic slices (A) Schematic representation of the [Ca^{2+}] time series projection snapshot and IF image overlay in an islet from a pancreatic slice **(B))** Comparison of α-cell volume fraction of 1st and last responders in the 1st stimulation (n = 74 1st responders and n = 74 last responders from 7 islets) (Mann-Whitney test was used for statistical analysis) **(C)** Experimental protocol and representative [Ca^{2+}] time course of an ex-9-treated islet in a live pancreatic slice **(D)** Comparison of the percentage decrease in islet-average 1st-phase peak amplitude during the 2nd stimulation in control and ex-9-treated islets (n = 4 control islets and n = 3 ex-9-treated islets) (Mann-Whitney test was used for statistical analysis) **(E)** Comparison of the change in 1st-phase response time of individual β-cells in control and ex-9-treated islets (control: n = 228 cells from 4 islets; ex-9-treated: n = 490 cells from 4 islets) (Mann-Whitney test was used for statistical analysis) **(F)** Comparison of α-cell volume fraction of 1st responders in the 1st and 2nd stimulations in control and ex-9-treated islets (control: n = 25 cells from 4 islets; ex-9 treated: n = 53 cells from 4 islets) (Mann-Whitney test was used for statistical analysis) (Experiments were performed in pancreatic slices for the data presented in this figure)

Figure 3. Variation in heterogeneity of 1st phase response time on blocking α-β communication (A) Visualization of heterogeneity of cell-wise 1st phase T_{resp} (red represents the islet with the highest variance, and blue represents the islet with the least variance in T_{resp}) **(B)** Comparison of islet-average variance of T_{resp} delay distributions between the 1st and 2nd stimulations in control and ex-9 treated islets (control: n = 8 islets, ex-9: 11 islets) (Wilcoxon matched-pairs signed-rank test was used for statistical analysis) **(C)** Comparison of difference in the range of time-of-response distributions (computed for each islet) of 1st and 2nd stimulations between control and ex-9 treated islets (control: n = 8 islets, ex-9: n = 11 islets) (Mann-Whitney test was used for statistical analysis) **(D)** Schematic representation of independently responding 'domains' in a representative islet **(E)** Relationship between T_{resp} and distance to the local 1st responder of domain 1 (from Fig. 3D) for all cells in the domain **(F)** Comparison of speed of [Ca^{2+}] signal propagation in various domains between 1st and 2nd stimulations in control and ex-9 treated islets (control: n = 8 islets, ex-9: n = 10 islets) (Mann-Whitney test was used for statistical analysis, and outliers were removed using the ROUT method (Q = 1%)) **(F)** Comparison of the area of the domains between 1st and 2nd stimulations in control and ex-9 treated islets (control: n = 4 islets, ex-9: n = 4 islets) (Mann-Whitney test was used for statistical analysis) (Experiments were performed in isolated islets for the data presented in this figure).

Figure 4. Variation in oscillation frequency with α-cell proximity and ex-9 addition (A) Schematic representation of α- and δ- cells segmented from IF images of glucagon and somatostatin in Imaris **(B)** Relationship between the islet-average frequency of 2nd phase [Ca^{2+}] oscillations and number of α-cells in different islets (n = 12 islets, 5 from isolated islets and 7 from pancreatic slices) (Simple linear regression was used for statistical analysis) **(C)** Schematic representation of the windows used for frequency and functional network analysis in the 1st and 2nd stimulations **(D)** Comparison of change in cell-wise oscillation frequency between 1st and 2nd stimulations in control and ex-9 treated islets (control n = 87 cells from 4 islets, ex-9: n = 110 cells from 4 islets) (Mann-Whitney test was used for statistical analysis) **(E)** Schematic representation of [Ca^{2}] time series projection, 3D IF image with α-cells segmented in Imaris, and heatmap representing change in oscillation frequency in a representative control islet **(F)** Comparison of change in cell-wise oscillation frequencies (2nd – 1st stimulations) between α-neighboring and non α-neighboring β-cells in control islets (n = 43 non α-neighboring and n = 44 α-neighboring β-cells from 4 islets, and outliers were removed using the ROUT

method (Q = 1%)) (Mann-Whitney test was used for statistical analysis) **(G)** Schematic representation of [Ca^2] time series projection, 3D IF image with α-cells segmented in Imaris, and heatmap representing change in oscillation frequency in a representative ex-9 treated islet **(H)** Comparison of change in cell-wise oscillation frequencies (2nd – 1st stimulations) between α-neighboring and non α-neighboring β-cells in ex-9 treated islets (n = 86 non α-neighboring and n = 24 α-neighboring β-cells from 4 islets) (Mann-Whitney test was used for statistical analysis, and outliers were removed using the ROUT method (Q = 1%)) (Experiments were performed in pancreatic slices for the data presented in this figure, however, panel **(D)** includes data from both isolated islets and islets from slices) (Note: Only cells with (var(signal) > 0.25σ(noise)) were utilized for frequency analysis of the data presented in this figure)

Figure 5. Variation in functional connectivity with α-cell proximity and ex-9 addition (A) Functional networks in the 1st and 2nd stimulations in a representative control islet **(B)** Functional network in the 1st and 2nd stimulations in a representative ex-9 treated islet **(C)** Comparison of cell-wise change in the number of cells each cell is linked to (k_{avg}) in the 2nd stimulation on control and ex-9 addition (control: n = 228 cells from 4 islets, ex-9: n = 498 cells from 4 islets) (Mann-Whitney test was used for statistical analysis) **(D)** Comparison of change in standard deviation of cell-wise oscillation frequencies in control and ex-9 treated islets (control n = 4 islets, ex-9: n = 4 islets) (Mann-Whitney test was used for statistical analysis) (**E)** Comparison of the islet-wise proportion of hubs in the 2nd stimulation that were part of the same cell, 1st nearest neighbor, or 2nd nearest neighbor (same cell cluster) versus the proportion of hubs who were different cells in the 1st stimulation, in control and ex-9-treated islets (in panel **(F)**) (control: n = 4 islets, ex-9: n = 4 islets) (Wilcoxon matched-pairs signed-rank test was used for statistical analysis) **(G)** Comparison of islet-wise hub- and non-hub α-cell volume fraction (hubs and non-hubs identified in the 1st stimulation) (n = 8 islets) (Wilcoxon matched-pairs signed-rank test was used for statistical analysis) **(H)** Comparison of islet-wise fold change in hub-cell α-cell volume fraction in the 2nd stimulation in control and ex-9 treated islets (control: n = 4 islets, ex-9: n = 4 islets) (Mann-Whitney test was used for statistical analysis) **(I)** Comparison of cell-wise change in the relative connectivity rank (ranked using percentiles based on descending order of number of links) of α-neighboring β-cells between 1st and 2nd stimulations in control and ex-9 treated islets (control: n = 80 cells, ex-9 n = 74 cells) (Mann-Whitney test was used for statistical analysis) (Experiments were performed in pancreatic slices for the data presented in this figure) (Note: Only cells with (var(signal) > 0.125σ(noise)) were utilized for plotting frequency distribution in panel **(D)**)

References:

1. Benninger RKP, Kravets V: The physiological role of β-cell heterogeneity in pancreatic islet function. Nature Reviews Endocrinology 2022;18:9-22
2. Farnsworth NL, Hemmati A, Pozzoli M, Benninger RKP: Fluorescence recovery after photobleaching reveals regulation and distribution of connexin36 gap junction coupling within mouse islets of Langerhans. The Journal of Physiology 2014;592:4431-4446
3. Salomon D, Meda P: Heterogeneity and contact-dependent regulation of hormone secretion by individual B cells. Experimental Cell Research 1986;162:507-520
4. Katsuta H, Aguayo-Mazzucato C, Katsuta R, Akashi T, Hollister-Lock J, Sharma AJ, Bonner-Weir S, Weir GC: Subpopulations of GFP-Marked Mouse Pancreatic β-Cells Differ in Size, Granularity, and Insulin Secretion. Endocrinology 2012;153:5180-5187
5. Karaca M, Castel J, Tourrel-Cuzin C, Brun M, Géant A, Dubois M, Catesson S, Rodriguez M, Luquet S, Cattan P, Lockhart B, Lang J, Ktorza A, Magnan C, Kargar C: Exploring Functional β-Cell Heterogeneity In Vivo Using PSA-NCAM as a Specific Marker. PLOS ONE 2009;4:e5555

6. Kravets V, Dwulet JM, Schleicher WE, Hodson DJ, Davis AM, Pyle L, Piscopio RA, Sticco-Ivins M, Benninger RKP: Functional architecture of pancreatic islets identifies a population of first responder cells that drive the first-phase calcium response. PLoS Biol 2022;20:e3001761
7. Johnston Natalie R, Mitchell Ryan K, Haythorne E, Pessoa Maria P, Semplici F, Ferrer J, Piemonti L, Marchetti P, Bugliani M, Bosco D, Berishvili E, Duncanson P, Watkinson M, Broichhagen J, Trauner D, Rutter Guy A, Hodson David J: Beta Cell Hubs Dictate Pancreatic Islet Responses to Glucose. Cell Metabolism 2016;24:389-401
8. Salem V, Silva LD, Suba K, Georgiadou E, Neda Mousavy Gharavy S, Akhtar N, Martin-Alonso A, Gaboriau DCA, Rothery SM, Stylianides T, Carrat G, Pullen TJ, Singh SP, Hodson DJ, Leclerc I, Shapiro AMJ, Marchetti P, Briant LJB, Distaso W, Ninov N, Rutter GA: Leader β-cells coordinate Ca2+ dynamics across pancreatic islets in vivo. Nature Metabolism 2019;1:615-629
9. Bader E, Migliorini A, Gegg M, Moruzzi N, Gerdes J, Roscioni SS, Bakhti M, Brandl E, Irmler M, Beckers J, Aichler M, Feuchtinger A, Leitzinger C, Zischka H, Wang-Sattler R, Jastroch M, Tschöp M, Machicao F, Staiger H, Häring H-U, Chmelova H, Chouinard JA, Oskolkov N, Korsgren O, Speier S, Lickert H: Identification of proliferative and mature β-cells in the islets of Langerhans. Nature 2016;535:430-434
10. Benninger RKP, Hodson DJ: New Understanding of β-Cell Heterogeneity and In Situ Islet Function. Diabetes 2018;67:537-547
11. Caicedo A: Paracrine and autocrine interactions in the human islet: More than meets the eye. Seminars in Cell & Developmental Biology 2013;24:11-21
12. Huising MO, van der Meulen T, Huang JL, Pourhosseinzadeh MS, Noguchi GM: The Difference δ-Cells Make in Glucose Control. Physiology 2018;33:403-411
13. Hartig SM, Cox AR: Paracrine signaling in islet function and survival. Journal of Molecular Medicine 2020;98:451-467
14. Arrojo e Drigo R, Jacob S, García-Prieto CF, Zheng X, Fukuda M, Nhu HTT, Stelmashenko O, Peçanha FLM, Rodriguez-Diaz R, Bushong E, Deerinck T, Phan S, Ali Y, Leibiger I, Chua M, Boudier T, Song S-H, Graf M, Augustine GJ, Ellisman MH, Berggren P-O: Structural basis for delta cell paracrine regulation in pancreatic islets. Nature Communications 2019;10:3700
15. Strowski MZ, Parmar RM, Blake AD, Schaeffer JM: Somatostatin Inhibits Insulin and Glucagon Secretion via Two Receptor Subtypes: An in Vitro Study of Pancreatic Islets from Somatostatin Receptor 2 Knockout Mice*. Endocrinology 2000;141:111-117
16. Cejvan K, Coy DH, Efendic S: Intra-Islet Somatostatin Regulates Glucagon Release via Type 2 Somatostatin Receptors in Rats. Diabetes 2003;52:1176-1181
17. Moens K, Flamez D, Van Schravendijk C, Ling Z, Pipeleers D, Schuit F: Dual glucagon recognition by pancreatic beta-cells via glucagon and glucagon-like peptide 1 receptors. Diabetes 1998;47:66-72
18. Marchetti P, Lupi R, Bugliani M, Kirkpatrick CL, Sebastiani G, Grieco FA, Del Guerra S, D'Aleo V, Piro S, Marselli L, Boggi U, Filipponi F, Tinti L, Salvini L, Wollheim CB, Purrello F, Dotta F: A local glucagon-like peptide 1 (GLP-1) system in human pancreatic islets. Diabetologia 2012;55:3262-3272
19. Holter MM, Saikia M, Cummings BP: Alpha-cell paracrine signaling in the regulation of beta-cell insulin secretion. Frontiers in Endocrinology 2022;13
20. Bru-Tari E, Oropeza D, Herrera PL: Cell Heterogeneity and Paracrine Interactions in Human Islet Function: A Perspective Focused in β-Cell Regeneration Strategies. Frontiers in Endocrinology 2021;11
21. Hughes JW, Cho JH, Conway HE, DiGruccio MR, Ng XW, Roseman HF, Abreu D, Urano F, Piston DW: Primary cilia control glucose homeostasis via islet paracrine interactions. Proceedings of the National Academy of Sciences 2020;117:8912-8923
22. Hill TG, Hill DJ: The Importance of Intra-Islet Communication in the Function and Plasticity of the Islets of Langerhans during Health and Diabetes. In *International Journal of Molecular Sciences*, 2024

23. Unger RH, Orci L: The essential role of glucagon in the pathogenesis of diabetes mellitus. Lancet 1975;1:14-16
24. Lee YH, Wang M-Y, Yu X-X, Unger RH: Glucagon is the key factor in the development of diabetes. Diabetologia 2016;59:1372-1375
25. Baron AD, Schaeffer L, Shragg P, Kolterman OG: Role of Hyperglucagonemia in Maintenance of Increased Rates of Hepatic Glucose Output in Type II Diabetics. Diabetes 1987;36:274-283
26. Balasenthilkumaran NV, Whitesell JC, Pyle L, Friedman RS, Kravets V: Network approach reveals preferential T-cell and macrophage association with α-linked β-cells in early stage of insulitis in NOD mice. Frontiers in Network Physiology 2024;4
27. Anquetil F, Sabouri S, Thivolet C, Rodriguez-Calvo T, Zapardiel-Gonzalo J, Amirian N, Schneider D, Castillo E, Lajevardi Y, von Herrath MG: Alpha cells, the main source of IL-1β in human pancreas. J Autoimmun 2017;81:68-73
28. Benkahla MA, Sabouri S, Kiosses WB, Rajendran S, Quesada-Masachs E, von Herrath MG: HLA class I hyper-expression unmasks beta cells but not alpha cells to the immune system in pre-diabetes. Journal of Autoimmunity 2021;119:102628
29. Nunemaker CS, Zhang M, Wasserman DH, McGuinness OP, Powers AC, Bertram R, Sherman A, Satin LS: Individual Mice Can Be Distinguished by the Period of Their Islet Calcium Oscillations : Is There an Intrinsic Islet Period That Is Imprinted In Vivo? Diabetes 2005;54:3517-3522
30. Nunemaker CS, Wasserman DH, McGuinness OP, Sweet IR, Teague JC, Satin LS: Insulin secretion in the conscious mouse is biphasic and pulsatile. Am J Physiol Endocrinol Metab 2006;290:E523-529
31. Curry DL, L. BL, Grodsky GM: Dynamics of Insulin Secretion by the Perfused Rat Pancreas. Endocrinology 1968;83:572-584
32. Porte D, Pupo AA: Insulin responses to glucose: evidence for a two pool system in man. J Clin Invest 1969;48:2309-2319
33. Henquin J-C: Relative Importance of Extracellular and Intracellular Calcium for the Two Phases of Glucose-Stimulated Insulin Release: Studies with Theophylline*. Endocrinology 1978;102:723-730
34. Benninger RKP, Zhang M, Head WS, Satin LS, Piston DW: Gap Junction Coupling and Calcium Waves in the Pancreatic Islet. Biophysical Journal 2008;95:5048-5061
35. Ravier MA, Güldenagel M, Charollais A, Gjinovci A, Caille De, Söhl G, Wollheim CB, Willecke K, Henquin J-C, Meda P: Loss of Connexin36 Channels Alters β-Cell Coupling, Islet Synchronization of Glucose-Induced Ca2+ and Insulin Oscillations, and Basal Insulin Release. Diabetes 2005;54:1798-1807
36. Serre-Beinier V, Le Gurun S, Belluardo N, Trovato-Salinaro A, Charollais A, Haefliger JA, Condorelli DF, Meda P: Cx36 preferentially connects beta-cells within pancreatic islets. Diabetes 2000;49:727-734
37. Zmazek J, Klemen MS, Markovič R, Dolenšek J, Marhl M, Stožer A, Gosak M: Assessing Different Temporal Scales of Calcium Dynamics in Networks of Beta Cell Populations. Frontiers in Physiology 2021;12
38. Stožer A, Gosak M, Dolenšek J, Perc M, Marhl M, Rupnik MS, Korošak D: Functional connectivity in islets of Langerhans from mouse pancreas tissue slices. PLoS Comput Biol 2013;9:e1002923
39. Stožer A, Šterk M, Paradiž Leitgeb E, Markovič R, Skelin Klemen M, Ellis CE, Križančić Bombek L, Dolenšek J, MacDonald PE, Gosak M: From isles of königsberg to islets of Langerhans: Examining the function of the endocrine pancreas through network science. Front Endocrinol (Lausanne) 2022;13:922640
40. Kravets V, Levitt CH, Benninger RK: 195-OR: To Which Degree Do Alpha Cells Shape the Role of the Beta Cells First Responders? Diabetes 2023;72

41. Ren H, Li Y, Han C, Yu Y, Shi B, Peng X, Zhang T, Wu S, Yang X, Kim S, Chen L, Tang C: Pancreatic α and β cells are globally phase-locked. Nat Commun 2022;13:3721
42. Briggs JK, Gresch A, Marinelli I, Dwulet JM, Albers DJ, Kravets V, Benninger RKP: β-cell intrinsic dynamics rather than gap junction structure dictates subpopulations in the islet functional network. Elife 2023;12
43. Suba K, Patel Y, Martin-Alonso A, Hansen B, Xu X, Roberts A, Norton M, Chung P, Shrewsbury J, Kwok R, Kalogianni V, Chen S, Liu X, Kalyviotis K, Rutter GA, Jones B, Minnion J, Owen BM, Pantazis P, Distaso W, Drucker DJ, Tan TM, Bloom SR, Murphy KG, Salem V: Intra-islet glucagon signalling regulates beta-cell connectivity, first-phase insulin secretion and glucose homoeostasis. Mol Metab 2024;85:101947
44. Capozzi ME, Svendsen B, Encisco SE, Lewandowski SL, Martin MD, Lin H, Jaffe JL, Coch RW, Haldeman JM, MacDonald PE, Merrins MJ, D'Alessio DA, Campbell JE: β Cell tone is defined by proglucagon peptides through cAMP signaling. JCI Insight 2019;4
45. Svendsen B, Larsen O, Gabe MBN, Christiansen CB, Rosenkilde MM, Drucker DJ, Holst JJ: Insulin Secretion Depends on Intra-islet Glucagon Signaling. Cell Rep 2018;25:1127-1134.e1122
46. Capozzi ME, Wait JB, Koech J, Gordon AN, Coch RW, Svendsen B, Finan B, D'Alessio DA, Campbell JE: Glucagon lowers glycemia when β-cells are active. JCI Insight 2019;5
47. Tian G, Sandler S, Gylfe E, Tengholm A: Glucose- and hormone-induced cAMP oscillations in α- and β-cells within intact pancreatic islets. Diabetes 2011;60:1535-1543
48. Stožer A, Paradiž Leitgeb E, Pohorec V, Dolenšek J, Križančić Bombek L, Gosak M, Skelin Klemen M: The Role of cAMP in Beta Cell Stimulus-Secretion and Intercellular Coupling. Cells 2021;10
49. Wan QF, Dong Y, Yang H, Lou X, Ding J, Xu T: Protein kinase activation increases insulin secretion by sensitizing the secretory machinery to Ca2+. J Gen Physiol 2004;124:653-662
50. Kasai H, Hatakeyama H, Ohno M, Takahashi N: Exocytosis in islet beta-cells. Adv Exp Med Biol 2010;654:305-338
51. Light PE, Manning Fox JE, Riedel MJ, Wheeler MB: Glucagon-like peptide-1 inhibits pancreatic ATP-sensitive potassium channels via a protein kinase A- and ADP-dependent mechanism. Mol Endocrinol 2002;16:2135-2144
52. Shibasaki T, Takahashi H, Miki T, Sunaga Y, Matsumura K, Yamanaka M, Zhang C, Tamamoto A, Satoh T, Miyazaki J, Seino S: Essential role of Epac2/Rap1 signaling in regulation of insulin granule dynamics by cAMP. Proc Natl Acad Sci U S A 2007;104:19333-19338
53. Leech CA, Chepurny OG, Holz GG: Epac2-dependent rap1 activation and the control of islet insulin secretion by glucagon-like peptide-1. Vitam Horm 2010;84:279-302
54. Lu M, Wheeler MB, Leng XH, Boyd AE, 3rd: The role of the free cytosolic calcium level in beta-cell signal transduction by gastric inhibitory polypeptide and glucagon-like peptide I(7-37). Endocrinology 1993;132:94-100
55. Holz GG, Leech CA, Heller RS, Castonguay M, Habener JF: cAMP-dependent mobilization of intracellular Ca2+ stores by activation of ryanodine receptors in pancreatic beta-cells. A Ca2+ signaling system stimulated by the insulinotropic hormone glucagon-like peptide-1-(7-37). J Biol Chem 1999;274:14147-14156
56. Islam MS: The ryanodine receptor calcium channel of beta-cells: molecular regulation and physiological significance. Diabetes 2002;51:1299-1309
57. Kim BJ, Park KH, Yim CY, Takasawa S, Okamoto H, Im MJ, Kim UH: Generation of nicotinic acid adenine dinucleotide phosphate and cyclic ADP-ribose by glucagon-like peptide-1 evokes Ca2+ signal that is essential for insulin secretion in mouse pancreatic islets. Diabetes 2008;57:868-878
58. Kang G, Chepurny OG, Rindler MJ, Collis L, Chepurny Z, Li WH, Harbeck M, Roe MW, Holz GG: A cAMP and Ca2+ coincidence detector in support of Ca2+-induced Ca2+ release in mouse pancreatic beta cells. J Physiol 2005;566:173-188

59. Gromada J, Dissing S, Bokvist K, Renström E, Frøkjaer-Jensen J, Wulff BS, Rorsman P: Glucagon-like peptide I increases cytoplasmic calcium in insulin-secreting beta TC3-cells by enhancement of intracellular calcium mobilization. Diabetes 1995;44:767-774
60. Skelin Klemen M, Dolenšek J, Križančić Bombek L, Pohorec V, Gosak M, Slak Rupnik M, Stožer A: The effect of forskolin and the role of Epac2A during activation, activity, and deactivation of beta cell networks. Front Endocrinol (Lausanne) 2023;14:1225486
61. Shuai H, Xu Y, Ahooghalandari P, Tengholm A: Glucose-induced cAMP elevation in β-cells involves amplification of constitutive and glucagon-activated GLP-1 receptor signalling. Acta Physiol (Oxf) 2021;231:e13611
62. Aslanidi OV, Mornev OA, Skyggebjerg O, Arkhammar P, Thastrup O, Sørensen MP, Christiansen PL, Conradsen K, Scott AC: Excitation wave propagation as a possible mechanism for signal transmission in pancreatic islets of Langerhans. Biophys J 2001;80:1195-1209
63. Baltrusch S, Lenzen S: Regulation of [Ca2+]i oscillations in mouse pancreatic islets by adrenergic agonists. Biochem Biophys Res Commun 2007;363:1038-1043
64. Cane MC, Parrington J, Rorsman P, Galione A, Rutter GA: The two pore channel TPC2 is dispensable in pancreatic β-cells for normal Ca^{2+} dynamics and insulin secretion. Cell Calcium 2016;59:32-40
65. Zaborska KE, Jordan KL, Thorson AS, Dadi PK, Schaub CM, Nakhe AY, Dickerson MT, Lynch JC, Weiss AJ, Dobson JR, Jacobson DA: Liraglutide increases islet Ca. Diabetes Obes Metab 2022;24:1741-1752
66. Tengholm A, Gylfe E: cAMP signalling in insulin and glucagon secretion. Diabetes Obes Metab 2017;19 Suppl 1:42-53
67. Delgadillo-Silva LF, Tasöz E, Singh SP, Chawla P, Georgiadou E, Gompf A, Rutter GA, Ninov N: Optogenetic β cell interrogation in vivo reveals a functional hierarchy directing the Ca. Sci Adv 2024;10:eado4513
68. Peng X, Ren H, Yang L, Tong S, Zhou R, Long H, Wu Y, Wang L, Wu Y, Zhang Y, Shen J, Zhang J, Qiu G, Wang J, Han C, Zhang Y, Zhou M, Zhao Y, Xu T, Tang C, Chen Z, Liu H, Chen L: Readily releasable β cells with tight Ca2+–exocytosis coupling dictate biphasic glucose-stimulated insulin secretion. Nature Metabolism 2024;6:238-253
69. Zhang F, Zhang L, Qi Y, Xu H: Mitochondrial cAMP signaling. Cell Mol Life Sci 2016;73:4577-4590
70. Paradiž Leitgeb E, Pohorec V, Križančić Bombek L, Skelin Klemen M, Duh M, Gosak M, Dolenšek J, Stožer A: Calcium imaging and analysis in beta cells in acute mouse pancreas tissue slices. Methods Mol Biol 2025;2861:223-246
71. Stožer A, Dolenšek J, Križančić Bombek L, Pohorec V, Slak Rupnik M, Klemen MS: Confocal Laser Scanning Microscopy of Calcium Dynamics in Acute Mouse Pancreatic Tissue Slices. JoVE 2021:e62293
72. Stožer A, Dolenšek J, Rupnik MS: Glucose-Stimulated Calcium Dynamics in Islets of Langerhans in Acute Mouse Pancreas Tissue Slices. PLOS ONE 2013;8:e54638
73. Schneider CA, Rasband WS, Eliceiri KW: NIH Image to ImageJ: 25 years of image analysis. Nature Methods 2012;9:671-675
74. Schindelin J, Arganda-Carreras I, Frise E, Kaynig V, Longair M, Pietzsch T, Preibisch S, Rueden C, Saalfeld S, Schmid B, Tinevez J-Y, White DJ, Hartenstein V, Eliceiri K, Tomancak P, Cardona A: Fiji: an open-source platform for biological-image analysis. Nature Methods 2012;9:676-682
75. Šterk M, Dolenšek J, Skelin Klemen M, Križančić Bombek L, Paradiž Leitgeb E, Kerčmar J, Perc M, Slak Rupnik M, Stožer A, Gosak M: Functional characteristics of hub and wave-initiator cells in β cell networks. Biophys J 2023;122:784-801
76. Šterk M, Zhang Y, Pohorec V, Leitgeb EP, Dolenšek J, Benninger RKP, Stožer A, Kravets V, Gosak M: Network representation of multicellular activity in pancreatic islets: Technical

considerations for functional connectivity analysis. PLOS Computational Biology 2024;20:e1012130
77. Gosak M, Markovič R, Dolenšek J, Slak Rupnik M, Marhl M, Stožer A, Perc M: Network science of biological systems at different scales: A review. Physics of Life Reviews 2018;24:118-135
78. Zhang Q, Galvanovskis J, Abdulkader F, Partridge CJ, Göpel SO, Eliasson L, Rorsman P: Cell coupling in mouse pancreatic beta-cells measured in intact islets of Langerhans. Philos Trans A Math Phys Eng Sci 2008;366:3503-3523
79. Karlöf L, Ølgård TA, Godtliebsen F, Kaczmarska M, Fischer H: Statistical techniques to select detection thresholds for peak signals in ice-core data. Journal of Glaciology 2005;51:655-662

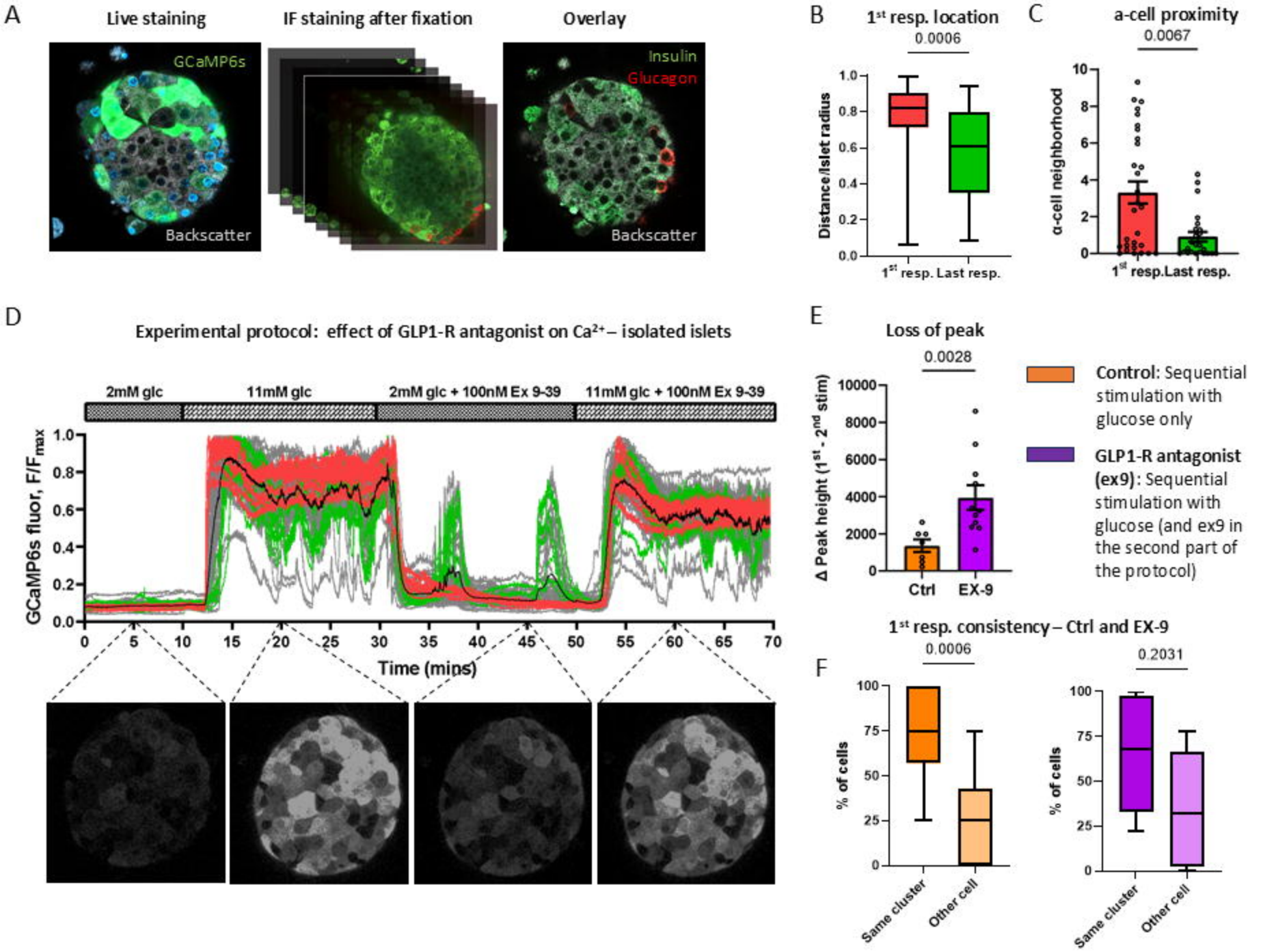
A
Live staining
IF staining after fixation
Overlay
GCaMP6s
Backscatter
Insulin
Glucagon
Backscatter
B
1st resp. location
0.0006
Distance/Islet radius
1st resp.
Last resp.
C
a-cell proximity
0.0067
α-cell neighborhood
1st resp.
Last resp.
D
Experimental protocol: effect of GLP1-R antagonist on Ca2+– isolated islets
2mM glc
11mM glc
2mM glc + 100nM Ex 9-39
11mM glc + 100nM Ex 9-39
GCaMP6s fluor, F/Fmax
Time (mins)
E
Loss of peak
0.0028
Δ Peak height (1st - 2nd stim)
Ctrl
EX-9
Control: Sequential stimulation with glucose only
GLP1-R antagonist (ex9): Sequential stimulation with glucose (and ex9 in the second part of the protocol)
1st resp. consistency – Ctrl and EX-9
F
0.0006
0.2031
% of cells
Same cluster
Other cell

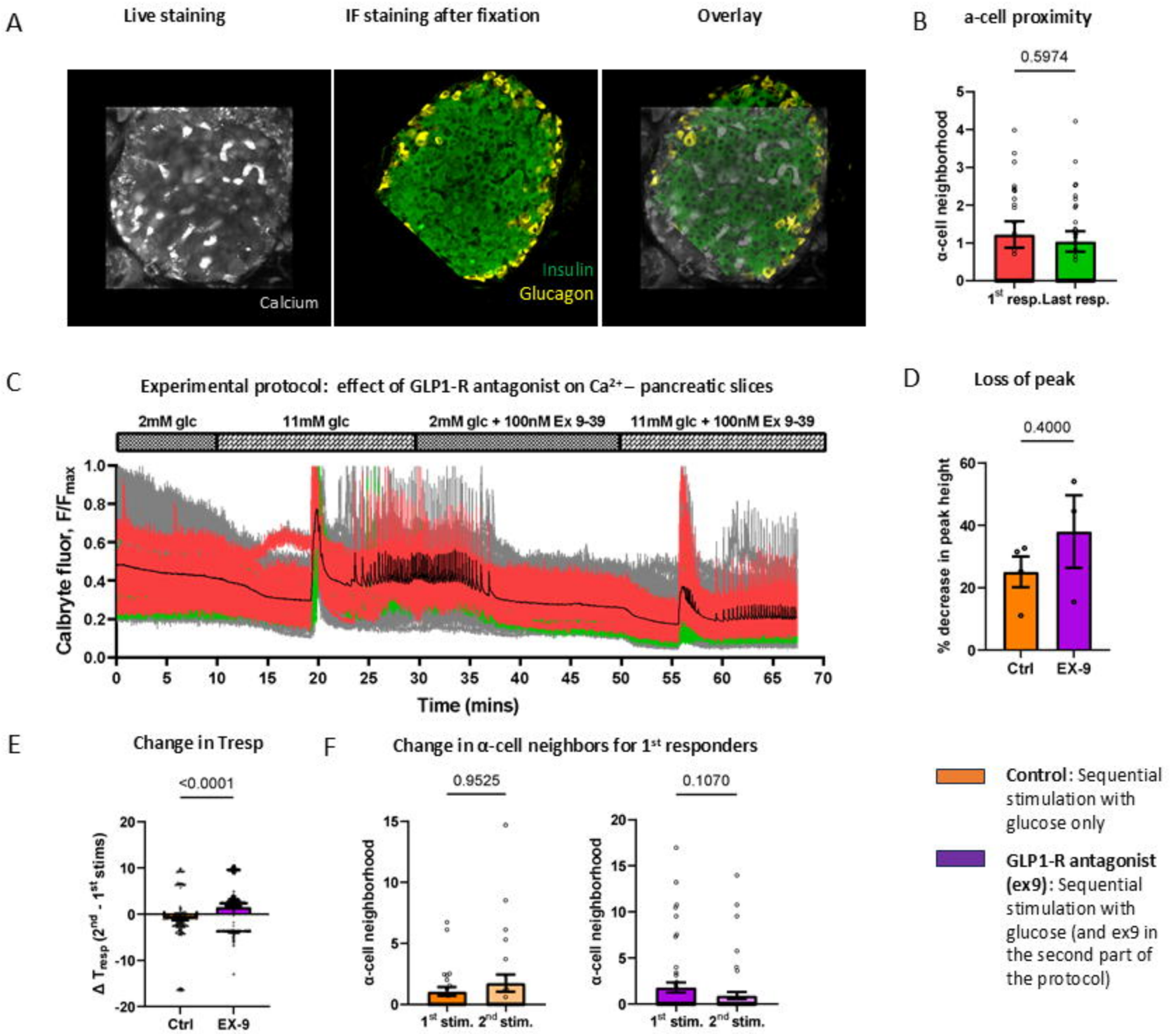
A
Live staining
IF staining after fixation
Overlay
Calcium
Insulin
Glucagon
B
a-cell proximity
0.5974
α-cell neighborhood
1st resp.
Last resp.
C
Experimental protocol: effect of GLP1-R antagonist on Ca2+– pancreatic slices
2mM glc
11mM glc
2mM glc + 100nM Ex 9-39
11mM glc + 100nM Ex 9-39
Calbryte fluor, F/Fmax
Time (mins)
D
Loss of peak
0.4000
% decrease in peak height
Ctrl
EX-9
E
Change in Tresp
<0.0001
Δ Tresp (2nd - 1st stims)
Ctrl
EX-9
F
Change in α-cell neighbors for 1st responders
0.9525
0.1070
α-cell neighborhood
1st stim.
2nd stim.
Control: Sequential stimulation with glucose only
GLP1-R antagonist (ex9): Sequential stimulation with glucose (and ex9 in the second part of the protocol)

A

Distributions of T_{resp} in the islets

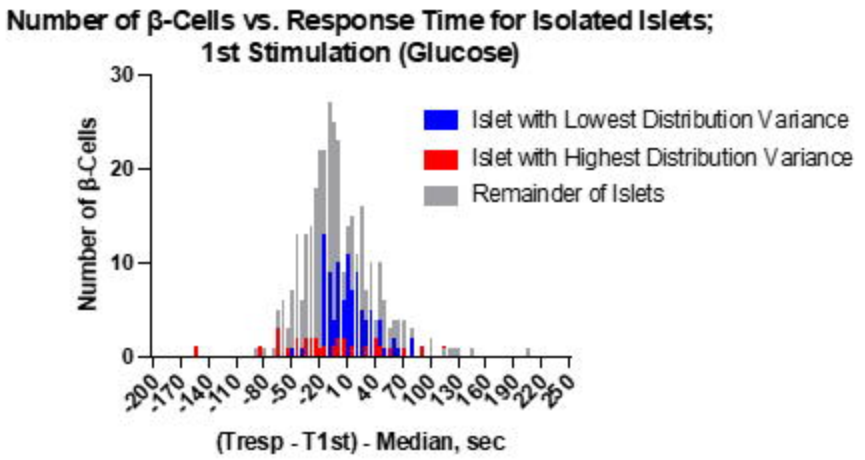

B

Change in the variance of T_{resp} distribution

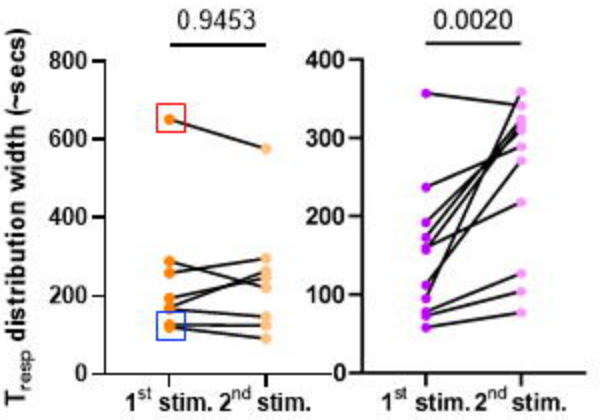

C

Change is T_{resp} distr. width

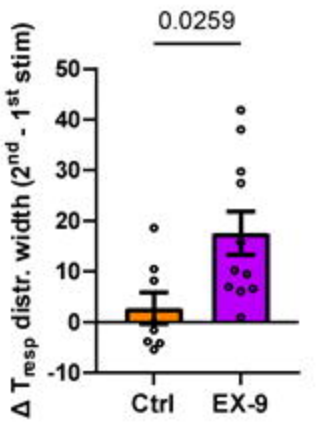

D

Color coded T_{resp}

Domain representation

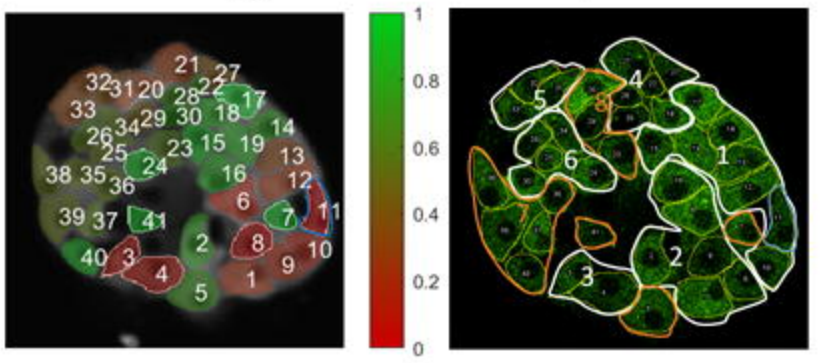

E

Speed of 1st phase recruitment signal propagation in a single domain

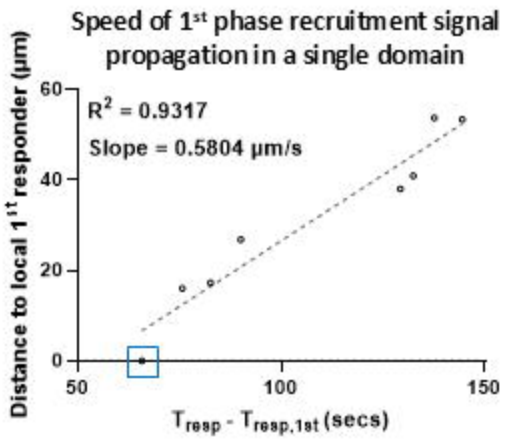

Control: Sequential stimulation with glucose only

GLP1-R antagonist (ex9): Sequential stimulation with glucose (and ex9 in the second part of the protocol)

F

Change in propagation speed – Ctrl and EX-9

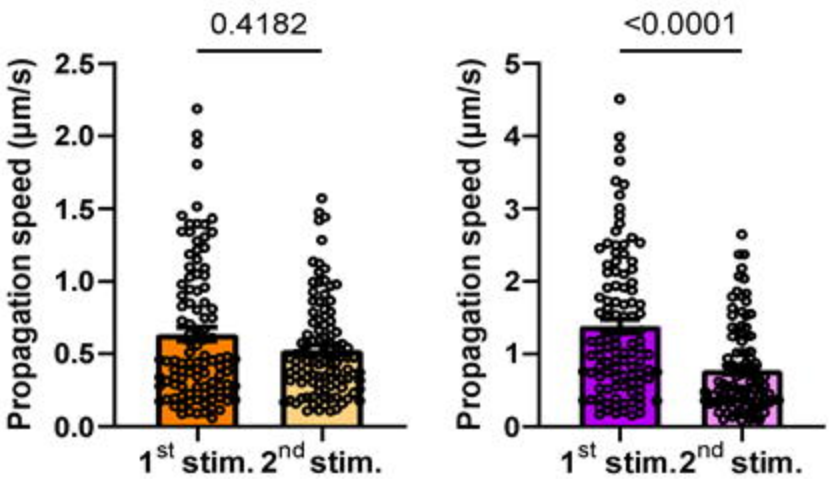

G

Change in domain area – Ctrl and EX-9

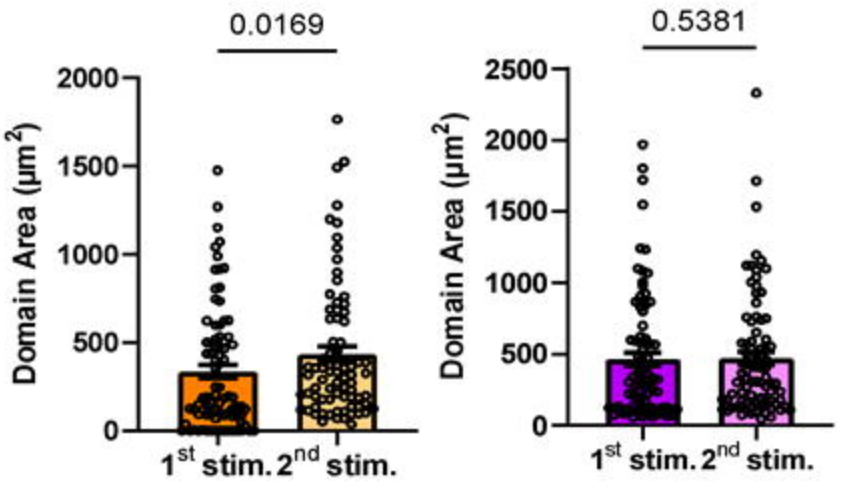

A

α- and δ-cell representation

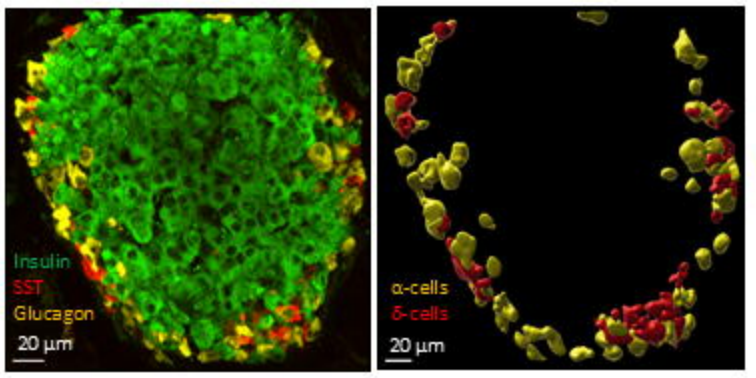

B

α-cell count vs frequency

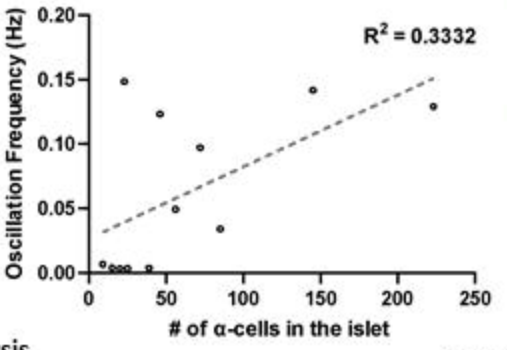

Control: Sequential stimulation with glucose only

GLP1-R antagonist (ex9): Sequential stimulation with glucose (and ex9 in the second part of the protocol)

C

Window selection for 2nd phase analysis

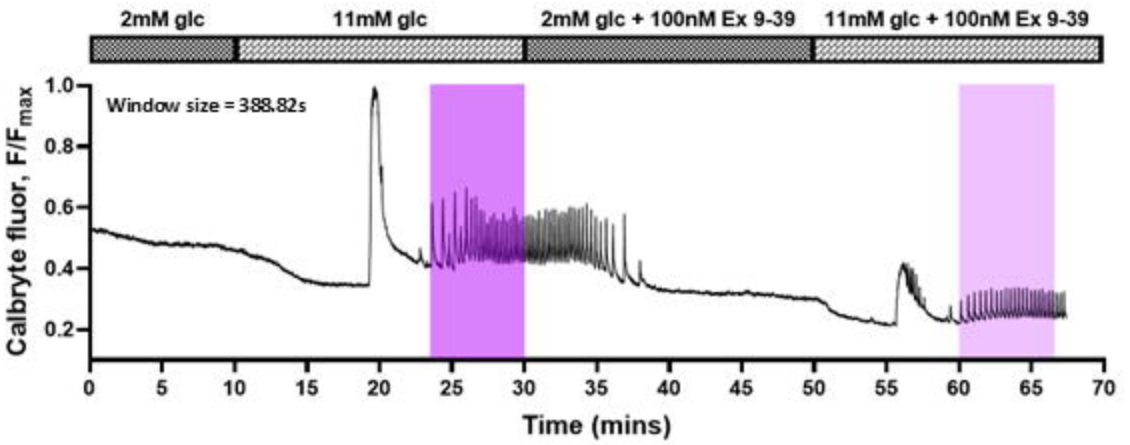

D

Δ Frequency between two stimulations

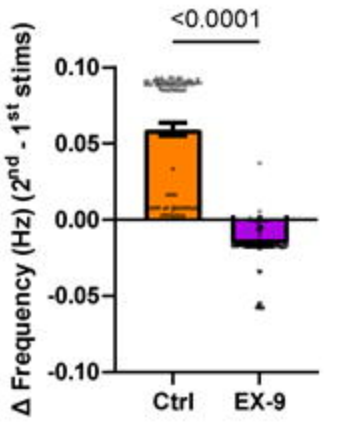

E

Control slices

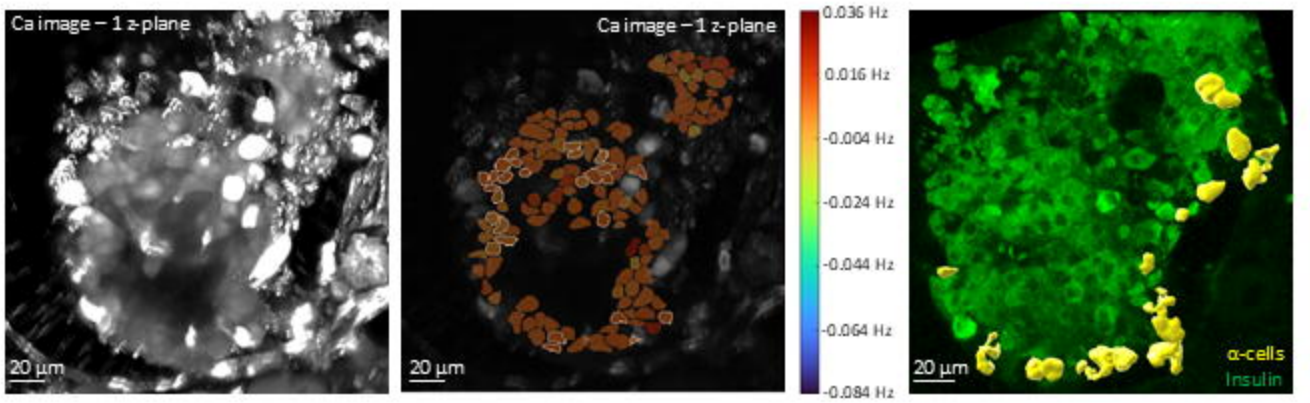

F

Δ Frequency w/ or w/o a-cell neighbors

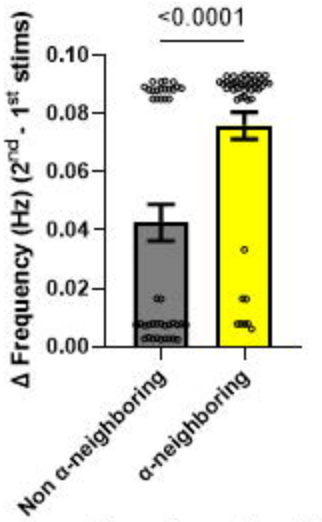

G

EX-9 treated slices

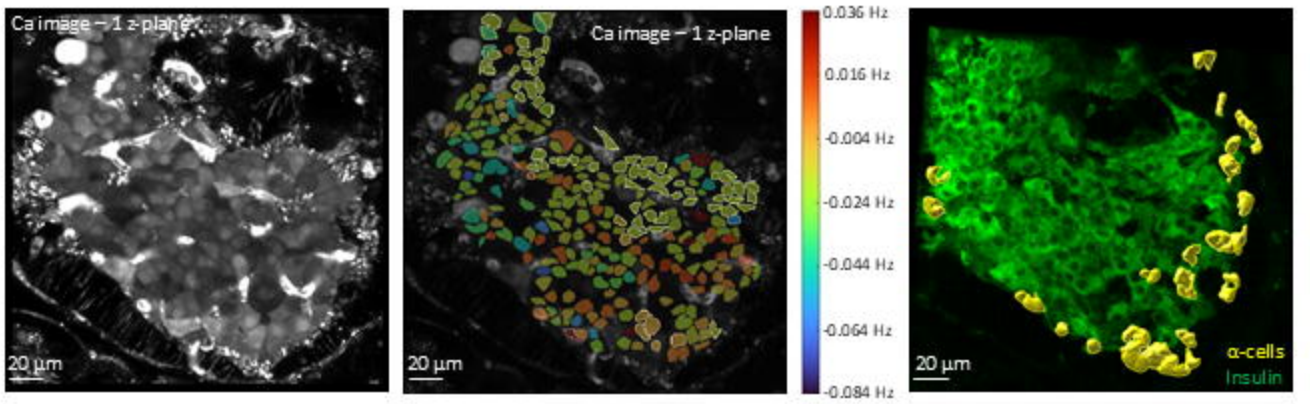

H

Δ Frequency w/ or w/o a-cell neighbors

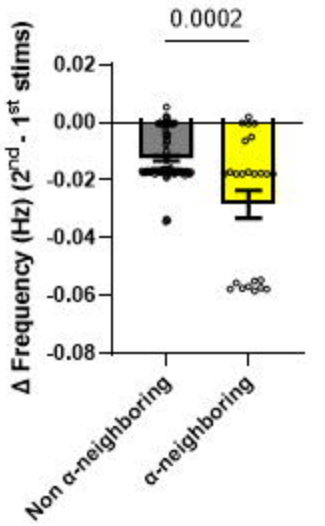

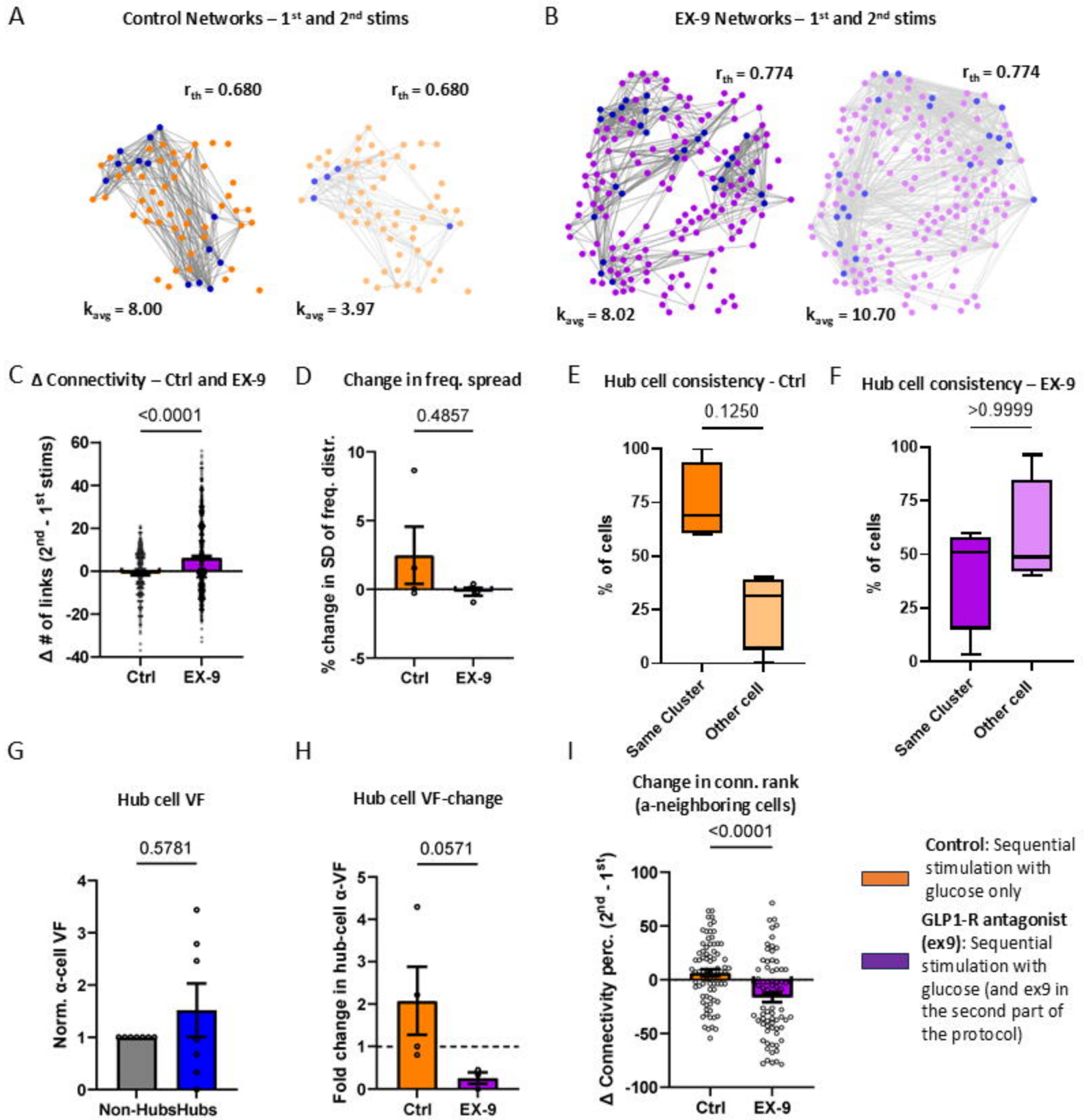
A
Control Networks – 1st and 2nd stims
r_{th} = 0.680
r_{th} = 0.680
k_{avg} = 8.00
k_{avg} = 3.97
B
EX-9 Networks – 1st and 2nd stims
r_{th} = 0.774
r_{th} = 0.774
k_{avg} = 8.02
k_{avg} = 10.70
C
Δ Connectivity – Ctrl and EX-9
<0.0001
Δ # of links (2nd - 1st stims)
Ctrl
EX-9
D
Change in freq. spread
0.4857
% change in SD of freq. distr.
Ctrl
EX-9
E
Hub cell consistency - Ctrl
0.1250
% of cells
Same Cluster
Other cell
F
Hub cell consistency – EX-9
>0.9999
% of cells
Same Cluster
Other cell
G
Hub cell VF
0.5781
Norm. α-cell VF
Non-Hubs
Hubs
H
Hub cell VF-change
0.0571
Fold change in hub-cell α-VF
Ctrl
EX-9
I
Change in conn. rank
(a-neighboring cells)
<0.0001
Δ Connectivity perc. (2nd - 1st stims)
Ctrl
EX-9
Control: Sequential stimulation with glucose only
GLP1-R antagonist (ex9): Sequential stimulation with glucose (and ex9 in the second part of the protocol)